# Spin pumping effects in Finemet|Pt and Finemet|Ta bilayers: Influence of real and imaginary part of spin mixing conductance on magnetization dynamics.

A. Krysztofik, H. Głowiński, I. Gościańska and J. Dubowik*

*Institute of Molecular Physics, Polish Academy of Sciences, M. Smoluchowskiego 17, 60-179 Poznań, Poland*

E. Coy, K. Załęski

*NanoBioMedical Centre, A. Mickiewicz University, Umultowska 18, 60-614 Poznań, Poland*

*dubowik@ifmpan.poznan.pl

## Abstract

We present the results of broadband ferromagnetic resonance studies on bilayers comprised of Finemet thin films covered by Pt and Ta wedge layers with the aim to observe spin pumping effects and to evaluate both the real and imaginary parts of the spin mixing conductance. The obtained experimental results are analyzed in the framework of a recent microscopic theory of spin pumping effects and confirm the important role of spin-orbit interactions at interfaces between Finemet and nonmagnetic heavy metal such as Pt and Ta. In particular, we show that the imaginary part of spin mixing conductance has comparable value to the real part and discuss its influence on magnetization dynamics.

## I. INTRODUCTION

Spin current flow across ferromagnet (FM)|non-magnetic metal (NM) is involved in spin pumping effects and leads to enhanced magnetization damping and a renormalized gyromagnetic ratio $\gamma$. The spin pumping effects can be detected by measuring the effective Gilbert damping constant or the spin transfer torque [1,2]. While an enhancement of the Gilbert damping constant due to spin pumping has been extensively studied enabling evaluation of the real part of spin mixing conductance $\mathrm{Re}\left[g_{eff}^{\uparrow\downarrow}\right]$ [3], changes of the gyromagnetic ratio (or the frequency of ferromagnetic resonance) were only scarcely mentioned since the imaginary part of spin mixing conductance $\mathrm{Im}\left[g_{eff}^{\uparrow\downarrow}\right]$ is regarded 1-2 order of magnitude smaller than the real part [4]. However, in the very first ferromagnetic resonance (FMR) experiment by Mizukami et al. [5] concerning the spin pumping effects, apparent changes in the gyromagnetic ratio (or the $g$-factor) were observed experimentally without comprehensive explanation.

From among few reports discussing the changes of the resonance field (or a "fieldlike" torque) in the context of spin pumping effects, it is worth to list a few in which either a field-shift or $\mathrm{Im}\left[g_{eff}^{\uparrow\downarrow}\right]$ were mentioned. By analyzing spin-orbit torque and spin pumping in NiFe|Pt bilayers, Nan et al. demonstrated that $\mathrm{Re}\left[g_{eff}^{\uparrow\downarrow}\right] = 2.2 \times 10^{15} cm^{-2}$ is only 3.7 times larger than $\mathrm{Im}\left[g_{eff}^{\uparrow\downarrow}\right] = 0.6 \times 10^{15} cm^{-2}$ [6]. They, however, have found that an additional contribution to damping at the NiFe|Pt interface distincts from the spin pumping. Sun et al. have found that a strong damping enhancement in YIG|Pt bilayers is accompanied by a shift in the resonance field [7]. They concluded that the spin pumping effects may originate partially from ferromagnetic ordering due to the magnetic proximity effect in Pt atomic layers near the interface. However, they have not linked the resonance field shift with $\mathrm{Im}\left[g_{eff}^{\uparrow\downarrow}\right]$. An elegant interpretation of the imaginary part of the spin mixing conductance generated by FM insulators with exchange-coupled local moments at the interface to a metal has been recently proposed by Cahaya et al. [8]. They assumed that a coherent motion of the proximity RKKY spin density (for example in Pt) is locked to the precessing magnetization of the local moments leading to a renormalization of the effective magnetic field. Moreover, for current-induced spin-orbit torques it was shown that the real part of the spin mixing conductance contributes to the damping-like torque while the imaginary part contributes to the field-like torque [9]. It is also important to point out that the field-like torque become lately the subject of discussion since experimental results concerning spin pumping systems suggested that it may play decisive role governing magnetization dynamics, although the values of $\mathrm{Im}\left[g_{eff}^{\uparrow\downarrow}\right]$ were not determined from the requisite measurements [10].

## II. MICROSCOPIC ANALYSIS OF SPIN PUMPING

Recently, a consistent analysis of spin pumping has been presented by Tatara and Mizukami [11] for both metallic and insulating ferromagnets. Let us summarize briefly the main results of their analysis. In the scattering approach the spin current pumped by FMR results in modification of the Gilbert damping coefficient $\alpha$ and the gyromagnetic ratio $\gamma$ via spin mixing conductance [12,13]:

$$\tilde{\alpha} = \alpha_0 + \frac{a^3}{4\pi S d_F}\mathrm{Re}\left[g_{eff}^{\uparrow\downarrow}\right] \tag{1}$$

and

$$\tilde{\gamma} = \gamma_0\left(1 - \frac{a^3}{4\pi S d_F}\mathrm{Im}\left[g_{eff}^{\uparrow\downarrow}\right]\right)^{-1}, \tag{2}$$

where $a$ is the lattice constant, $S$ is the magnitude of the localized spin, $d_F$ is the thickness of the ferromagnet. As $a^3/(4\pi S) = \hbar\gamma_0/4\pi M_S$ and $\gamma_0 = g_0\mu_B/\hbar$, where $M_S$ is the saturation magnetization, ħ is the reduced Planck constant and $\mu_B$ is the Bohr magneton, Eqs. (1) and (2) can be rewritten to

$$\delta\alpha = \tilde{\alpha} - \alpha_0 = \frac{g_0\mu_B}{4\pi M_S d_F}\mathrm{Re}\left[g_{eff}^{\uparrow\downarrow}\right] \tag{3}$$

and

$$\delta g/g_0 = (\tilde{g} - g_0)/g_0 \cong \frac{g_0\mu_B}{4\pi M_S d_F}\mathrm{Im}\left[g_{eff}^{\uparrow\downarrow}\right]. \tag{4}$$

Hence,

$$\frac{\delta\alpha}{\delta g/g_0} \cong \frac{\mathrm{Re}\left[g_{eff}^{\uparrow\downarrow}\right]}{\mathrm{Im}\left[g_{eff}^{\uparrow\downarrow}\right]} \tag{5}$$

and the ratio of $\mathrm{Re}\left[g_{eff}^{\uparrow\downarrow}\right]$ to $\mathrm{Im}\left[g_{eff}^{\uparrow\downarrow}\right]$ can be easily estimated from the spin-pumping experiments.

In the microscopic analysis, the magnetization dynamics is derived by evaluating the spin accumulation in a nonmagnetic metal as a result of interface hopping. One of the main consequences of the analysis [11] is an approximation of enhancement of the Gilbert damping constant:

$$\delta\alpha \sim \frac{a}{d_F}\frac{1}{\epsilon_F^2}\widetilde{t_\uparrow^0}\widetilde{t_\downarrow^0} \tag{6}$$

with the so-called hopping amplitudes $\widetilde{t_{\uparrow}^{0}}$ and $\widetilde{t_{\downarrow}^{0}}$, which have unit of energy. $\epsilon_F$ is the Fermi energy. Similarly, the change in the $g$-factor due to spin pumping can be rewritten from Eq. (84) in Ref. [11] to

$$\frac{\delta g}{g_0} \sim \frac{a}{d_F}\frac{1}{\epsilon_F^2}\tilde{\gamma}_{xz}\left(\widetilde{t_{\uparrow}^{0}} + \widetilde{t_{\downarrow}^{0}}\right), \tag{7}$$

where $\tilde{\gamma}_{xz}$ is a coefficient having the unit of energy representing the interface spin-orbit interaction. Equation (7) suggests that a high value of $\delta g/g_0$ is expected if strong interface spin-orbit interaction exists. Therefore, the ratio $\delta\alpha/(\delta g/g_0)$, which is accessible experimentally, can be approximated by

$$\frac{\delta\alpha}{\delta g/g_0} \cong \frac{\widetilde{t_{\uparrow}^{0}}\widetilde{t_{\downarrow}^{0}}}{\tilde{\gamma}_{xz}\left(\widetilde{t_{\uparrow}^{0}}+\widetilde{t_{\downarrow}^{0}}\right)}. \tag{8}$$

However, the ratio $\widetilde{t_{\uparrow}^{0}}/\widetilde{t_{\downarrow}^{0}}$ is not known a'priori so that we have to make a reasonable approximation by assuming that $\widetilde{t_{\uparrow}^{0}} + \widetilde{t_{\downarrow}^{0}} = \bar{t}$ and $\widetilde{t_{\uparrow}^{0}} = (1-n)\bar{t}$, $\widetilde{t_{\downarrow}^{0}} = n\bar{t}$, where $n$ is a number from the range of 0.1 … 0.9. Hence the expression (8) may be roughly approximated as

$$\frac{\delta\alpha}{\delta g/g_0} \cong 0.2\frac{\bar{t}}{\tilde{\gamma}_{xz}} \tag{9}$$

for $n = 0.3$, which is chosen as a mean number.

## III. SAMPLES STRUCTURE AND METHODS

To verify and experimentally examine the main results of the microscopic theory we fabricated F|NM bilayers using $Fe_{66.5}Cu_1Nb_3Si_{13.5}B_6Al_7$ (Finemet, F) for the ferromagnetic layer and Pt, Ta as a nonmagnetic metal (NM). Instead of commonly employed Permalloy films, we extensively used Finemet as a ferromagnet for the following reasons: (*i*) exceptional smoothness of Finemet surfaces [14]; (*ii*) smaller Gilbert damping constant in comparison to Permalloy [15,16]; (*iii*) relatively small inhomogeneous linewidth $\Delta H_0$ of 3-6 Oe indicating low density of defects [14].The Finemet films with different thicknesses were deposited at room temperature by pulsed laser deposition (base pressure of $8\times10^{-8}$ mbar) on naturally oxidized Si substrates and covered *in situ* with wedge-shaped capping layers of Pt or Ta ($0 < d_{NM} < 7$ nm) using RF magnetron sputtering. The nominal thicknesses of Finemet: $d_F = 10$, 15, 20, 30, 40 nm for the Pt cover layer and 2, 3.5, 5, 10 nm for Ta cover layer, were confirmed with X-ray reflectivity measurements, while thickness profiles of the NM capping layer were additionally verified using the energy dispersive spectroscopy in a scanning electron microscope. Atomic force microscopy measurements of Finemet surface yielded RMS roughness of 0.1 nm that is typical for amorphous films.

In order to determine structural properties of the films we conducted HR-TEM experiments and grazing incident X-ray diffraction. As shown in electron diffraction pattern (SAED) in Fig 1. (a), a diffuse ring marked in yellow is observed, indicating only the small occurrence of nanocrystalline or amorphous phase in the Finemet film. Apart from substrate peaks, reflections corresponding to a gold layer are visible, with which Finemet film was coated before the preparation of a cross-section by focused ion beam. The amorphous band corresponds roughly to the interplanar distance of 0.2±0.1 nm as presented in Fig. 1. (b), which was extracted by using rotational average of the Digitalmicrograph™, Diff tools

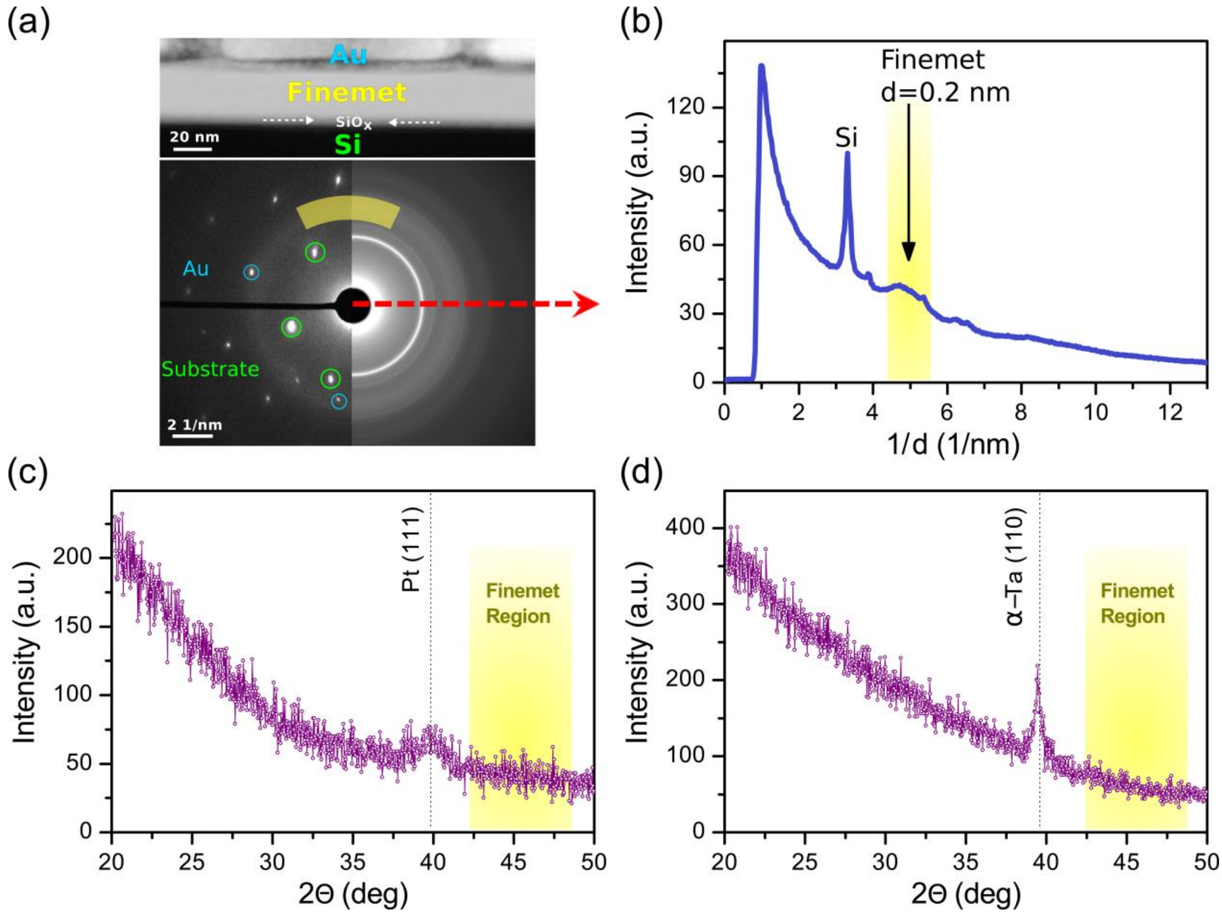


Fig. 1 (a) Low magnification scanning electron image of Finemet control layer (25 nm) coated *ex-situ* with Au for cross-section preparation, and the corresponding SAED pattern including both the substrate and the Au covering film (bottom panel). Dashed red arrow shows the direction of the profile taken from the rotational averaging, displayed in (b). The profile image shows the clear position of Finemet (d = 0.2 nm) plus the highly intense Si peaks. Finally, (c) and (d) shows the GiXRD spectra of Finemet (30nm) | Pt (6nm) and Finemet (10nm) | Ta (6nm) respectively, where the texture of Pt(111) and (d) α-Ta(110) covering layers can be seen.

plug-in [17]. This result is congruent with the simulation of Finemet unit cell (using the CaRIne Crystallography software, Lattice 2.8) yielding $d_{(110)}$=0.1980 nm. However, the highest intensity reflection (110), expected to be at 45.75 angle 2Θ, is not observed in grazing incident X-ray diffraction as marked by shaded areas in Fig. 1 (c) and (d). Nevertheless, these measurements allowed us to determine the structure of capping Pt and Ta layers. We conclude that the studied bilayer systems consist of amorphous or nanocrystalline Finemet films covered with α-Ta (i.e., bcc) or Pt with well-defined (110) and (111) texture, respectively.

Ferromagnetic resonance measurements of the samples were carried out at room temperature on a coplanar waveguide (CPW) in the in-plane configuration over a frequency range of 4 - 40 GHz, as detailed in Ref. [18,19]. For each thickness $d_{NM}$ we measured the field swept complex transmission parameter $S_{21}$(H) by placing the sample at a certain position along the wedge ( Fig.2(a)). The real and imaginary transmission spectra were fitted using the Lorenzian and anti-Lorentzian function in a similar way as described in Ref. [20]. From the fits, the resonance field $H_r$ and resonance linewidth $\Delta H$ (full width at half maximum) were evaluated at several frequencies $f$. In short, our method involves the use of a single sample with a fixed thickness $d_F$ wherein the capping layer is wedge shaped, so by scanning the sample over the central line of CPW one can determine parameters of magnetization dynamics as a function of $d_{NM}$. Such an approach is of crucial importance, because it eliminates the problem of the proper choice of a reference layer [21]. Since deposition conditions (and consequently film properties) may slightly differ in each sputtering or ablation process we have set the beginning of the NM wedge at 6-7 mm from the substrate's edge allowing for the measurements of a lone Finemet film in every F|NM bilayer (see the inset of Fig. 2 (a)).

## IV. EXPERIMENTAL RESULTS

Typical resonance spectra of Finemet (30 nm) | Pt (0 − 7 nm) sample, measured at $f = 7$ GHz for various positions along the wedge, are displayed in Fig. 2 (a). It can be seen that an increase in linewidth is also accompanied by a substantial, yet unexpected shift in the resonance field $H_r$ as the Pt thickness increases. The shift is negative (toward lower fields) and indicates systematical changes in the gyromagnetic ratio. To obtain values of the $g$-factor we performed fittings to $f$ vs $H_r$ dependences rather than evaluate changes in $H_r$ measured at one fixed frequency. As it is shown in Fig. 2 (b), the relation follows Kittel's dispersion $f = \frac{g\,\mu_B}{h}\sqrt{H_r(H_r + 4\pi M_{eff})}$, however detailed analysis of the fitting residuals revealed that

Finemet films possess non-negligible anisotropy field $H_a$ (see supplementary materials). Hence, the model was extended to the following expression:

$$f = \frac{g\,\mu_B}{h}\sqrt{(H_r + H_a)(H_r + H_a + 4\pi M_{eff})}, \tag{10}$$

where $M_{eff}$ is the effective magnetization. It should be emphasized that inclusion of $H_a$ in Eq. (10) (along with $g$-factor and $M_{eff}$) results in three, coupled adjustable parameters that are not orthogonal to each other during the least-squares non-linear fitting process [22]. Therefore, we followed methodology presented in Ref. [22] and applied asymptotic analysis to the data obtained over a finite range of frequencies in order to precisely determine the value of $g$-factor as presented below. Across the set of samples, we found that the Finemet films are characterized by $M_{eff}$ in the range of 750 ± 30 emu/cm$^3$ and $H_a$ in the range of 7 ± 2 Oe.

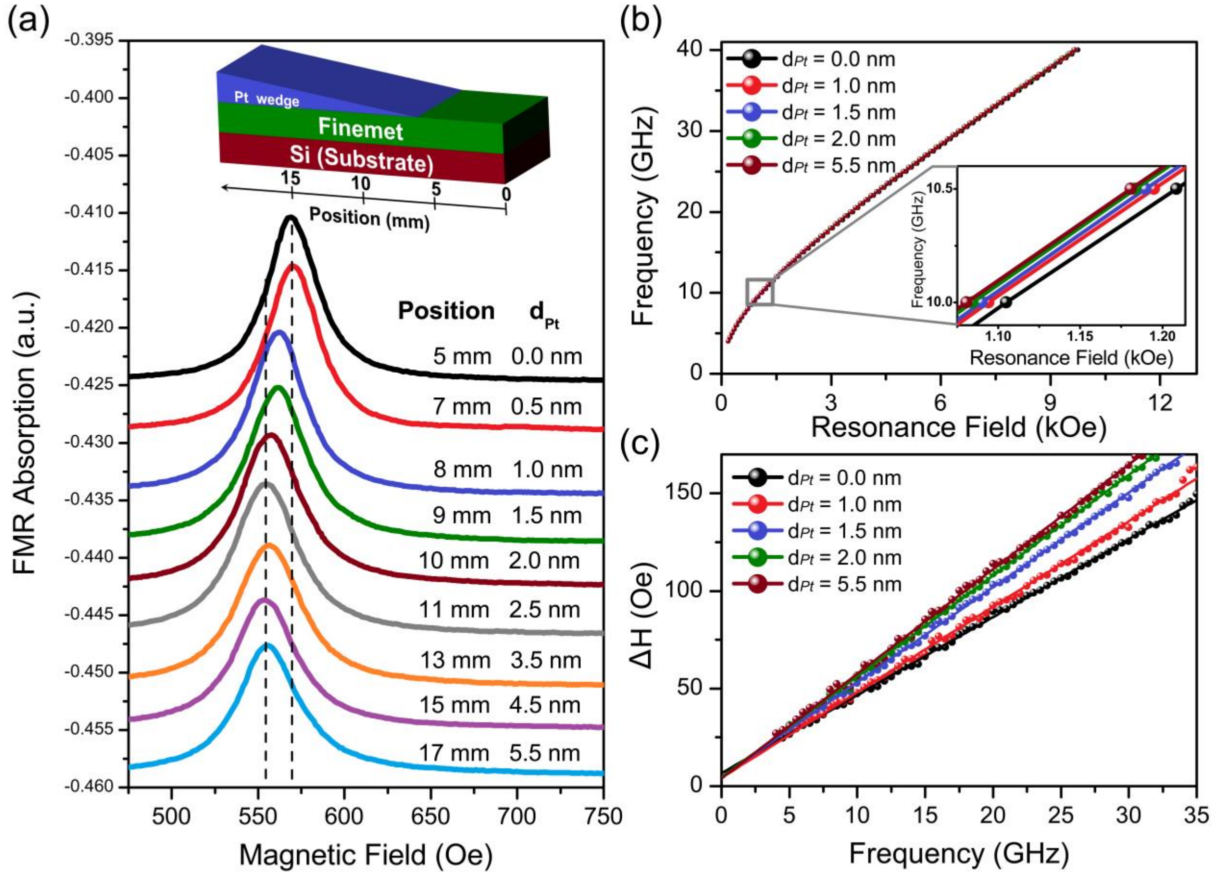


Fig. 2 VNA-FMR results for 30 nm thick Finemet film covered with Pt. (a) Typical FMR spectra taken at f = 7 GHz for various positions along the wedge-shaped Pt layer. (b) Frequency vs resonance field dependences fitted with Eq. (10). The inset shows enlarged region near f = 10 GHz. (c) Linewidth dependences on frequency fitted with Eq. (11).

Gilbert damping parameter $\alpha$ and inhomogeneous broadening $\Delta H_0$ for a given $d_F$ and different thicknesses $d_{NM}$ were obtained from linear fits to resonance linewidth $\Delta H$ as a function of frequency, according to the standard expression [23]:

$$\Delta H(f) = \frac{4\pi\alpha}{\gamma} f + \Delta H_0. \tag{11}$$

Even for relatively thick Finemet films (for example 30 nm as in Fig. 1 (c)) it is clearly seen that the slopes of $\Delta H(f)$ dependences experience a substantial change with increasing thickness of Pt. Indeed, as summarized in Fig. 3, continuous increase in the damping parameter $\alpha$ is observed for each investigated bilayer. The damping of a lone Finemet is equal to $\alpha = (5.8 \pm 0.3) \times 10^{-3}$, though for the thinnest sample (10 nm) it is slightly elevated to the value of $\alpha = (7.80 \pm 0.07) \times 10^{-3}$ [24]. The $\Delta H_0$ parameter remains below 10 Oe in the investigated set with the mean value of 6.4 Oe indicating low density of surface defects and, therefore, negligible extrinsic contributions to the linewidth

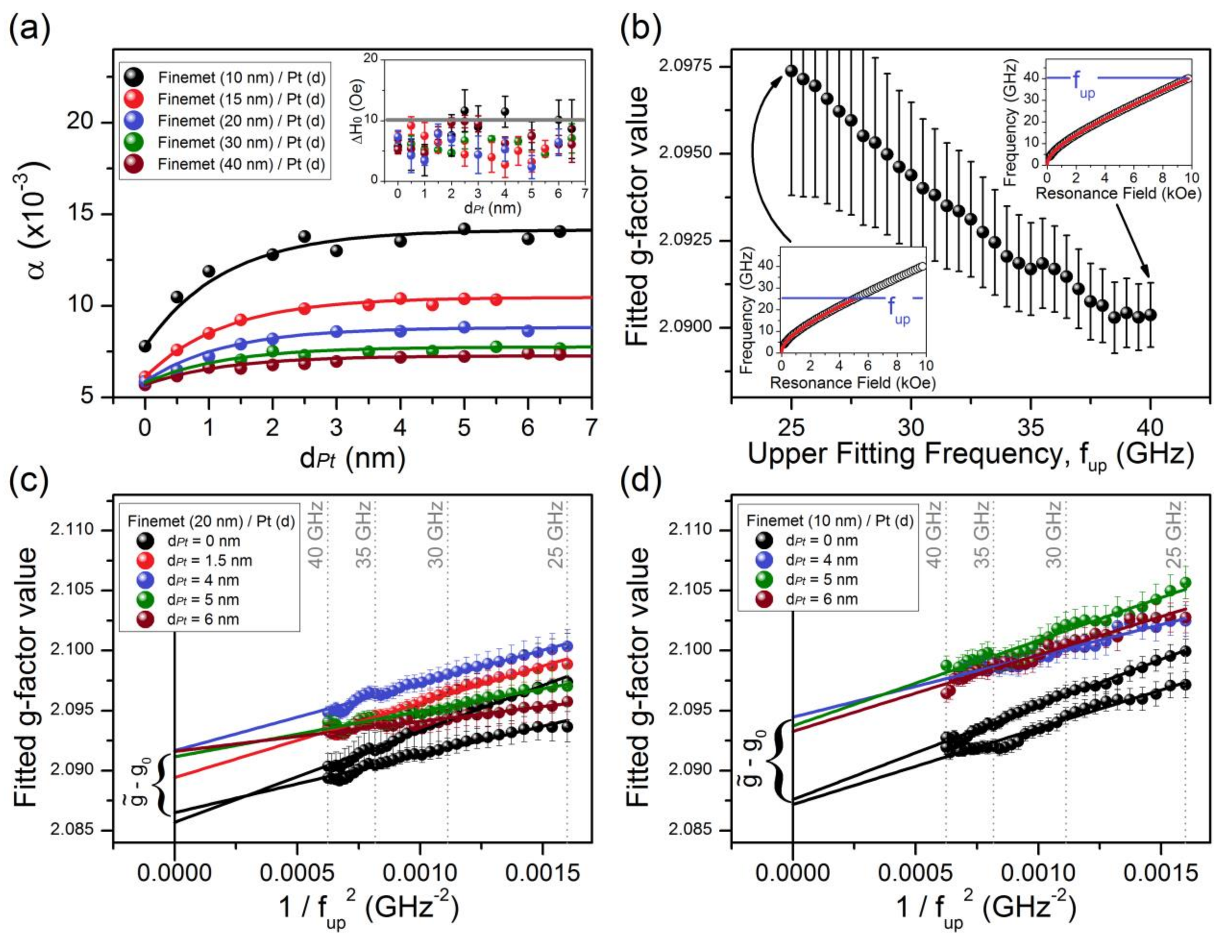


Fig. 3. (a) The Gilbert damping parameter $\alpha$ as a function of Pt film thickness. The solid lines were obtained by simultaneous fit to all collected data using Eq. (12). The inset shows values of $\Delta H_0$ parameter. (b) $g$-factor values of 20 nm thick Finemet fitted using Eq. (10) for different frequency ranges defined by $f_{up}$ as shown in the insets. In (c) and (d), the fitted values of $g$-factor are plotted as a function of $f_{up}^{-2}$ respectively for 20 nm and 10 nm thick Finemet with different Pt thicknesses $d_{Pt}$. Double sets of data for $d_{Pt} = 0$ nm (black symbols and lines) derive from measurements of the lone Finemet film taken at different positions outside the Pt wedge.

such as two-magnon scattering (inset in Fig 2(a)). Following the equation describing damping enhancement due to spin pumping [25]:

$$\alpha = \alpha_0 + \frac{g\mu_B}{4\pi M_S}\frac{\mathrm{Re}\left[g_{eff}^{\uparrow\downarrow}\right]}{d_F}(1-\exp(-\frac{2d_{NM}}{\lambda_{sf}})), \tag{12}$$

the real part of spin mixing conductance $\mathrm{Re}\left[g_{eff}^{\uparrow\downarrow}\right] = (3.14 \pm 0.23) \times 10^{15} cm^{-2}$, and additionally spin diffusion length $\lambda_{sf} = 2.8 \pm 0.5\ nm$ were obtained.

In order to determine the imaginary part of $g_{eff}^{\uparrow\downarrow}$, analysis of the $g$-factor was performed according to Eq. (4). First, the influence of finite fitting range on the obtained value of the $g$-factor was examined. As it is shown in Fig. 3 (b), with the increasing fitting range specified by the upper frequency $f_{up}$, the statistical error of the $g$-factor decreases and the value begin to saturate when plotted as a function of $f_{up}$. It is considered that for large enough resonance fields, fitted $g$-factor value becomes independent of the fitting range and therefore can be extrapolated from $g_{fit}\ (1/f_{up}^2)$ dependence [22]. Although this claim is not verifiable since every FMR spectrometer is limited either by available fields or frequencies, it should be highlighted that in terms of the analysis provided hereby, the method allows to reasonably determine the difference between $g$-factor values of the uncovered Finemet films and those capped with the non-magnetic metal. As can be seen in Fig. 3 (c) and (d), the difference $\delta g = \tilde{g} - g_0$ is essentially equivalent whether it is evaluated for $f_{up} = 40$ GHz or when $f_{up} \to \infty$ $(1/f_{up}^2 \to 0)$. However, taking into account the asymptotical values of $\tilde{g}$ and $g_0$ provide better statistical accuracy for such subtle changes in $g$-factor. For Platinum thickness equal to 1.5 nm (depicted by a red line in Fig. 3 (c)), it even allows for an observation of intermediate value of $g$-factor which falls between $\tilde{g}$ and $g_0$ and can be hardly concluded when the fitting is performed merely up to 40 GHz. This suggests that with the appearance of nonmagnetic layer, enhancement in $g$-factor does not occur in an immediate, step-like way but follows gradual increase until saturated. As it is presented in both Fig. 3 (c) and (d), asymptotically fitted $\tilde{g}$ for $d_{Pt} > 4$ nm already converge to nearly the same value. Moreover, the obtained difference $\delta g$ is greater for thinner Finemet film, congruently with the theoretical prediction given by Eq. (4). For the 20 nm thick Finemet $\delta g = (5.1 \pm 0.4) \times 10^{-3}$, while for 10 nm thick layer $\delta g = (6.7 \pm 0.4) \times 10^{-3}$. Such a result provides clear evidence of a spin pumping influence on magnetization dynamics expressed by the imaginary part of spin mixing conductance. Following this observation it is expected that the difference $\delta g$ will be larger for even thinner films. For the set of samples with Ta deposited on 2-10 nm thick

Finemet this influence is indeed much more pronounced as displayed in Fig. 4. Also quasi-linear enhancement in $g$-factor is observed as the thickness of Ta increases from 0 up to 2 nm.

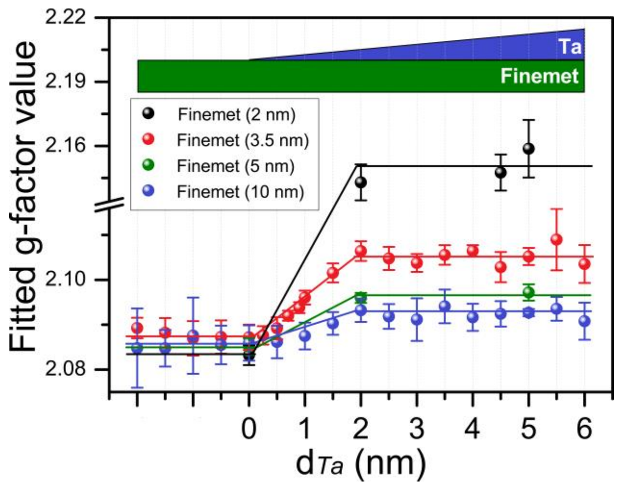


Fig. 4. Dependence of $g$-factor on Ta layer thickness for Finemet|Ta bilayers with $d_F = 2 - 10$ nm. Continuous lines serve as guides to the eye.

The main, experimental results of our paper are juxtaposed in Fig. 5, where $\delta\alpha$ and $\delta g/g_0$ are plotted versus the inverse thickness $d_F$ for Finemet|Pt and Finemet|Ta bilayers. The real and imaginary part of spin mixing conductance were determined from the slopes of linear fits according to Eqs. (3) and (4). For the sample covered with Platinum, $\mathrm{Re}[g_{eff}^{\uparrow\downarrow}] = (3.05 \pm 0.14) \times 10^{15} cm^{-2}$ in agreement with the value obtained above from simultaneous fit to the data presented in Fig. 3 (a). The $\mathrm{Im}[g_{eff}^{\uparrow\downarrow}]$ equals to $(1.69 \pm 0.22) \times 10^{15} cm^{-2}$, therefore the ratio $\mathrm{Re}[g_{eff}^{\uparrow\downarrow}]/\mathrm{Im}[g_{eff}^{\uparrow\downarrow}] = 1.81$ implies that the imaginary part of spin mixing conductance cannot be in general regarded as negligible in contrast to many common views [1,4,11]. Strikingly different relation is observed for Finemet film covered with Tantalum. It is clearly seen that the slope of $\delta g/g_0$ is substantially higher than the slope of $\delta\alpha$ vs $d_F^{-1}$. Here, $\mathrm{Re}[g_{eff}^{\uparrow\downarrow}] = (0.61 \pm 0.05) \times 10^{15} cm^{-2}$ and $\mathrm{Im}[g_{eff}^{\uparrow\downarrow}] = (1.61 \pm 0.07) \times 10^{15} cm^{-2}$, hence the ratio $\mathrm{Re}[g_{eff}^{\uparrow\downarrow}]/\mathrm{Im}[g_{eff}^{\uparrow\downarrow}] = 0.38$. It should be emphasized at this point that for the 2 nm-thick Finemet film ($1/d_F = 0.5\, nm^{-1}$) the value of $\delta g/g_0$ significantly deviates from the linear relationship as can be seen in Fig. 5(b). We found that in such thin film the saturation magnetization was decreased down to 450 ± 34 emu/cm$^3$ resulting in the augmented value of $\delta g/g_0$ (see the Eq. (4)). Therefore, in order to determine $\mathrm{Im}[g_{eff}^{\uparrow\downarrow}]$, the fitting was performed to $\delta g/g_0$vs $(4\pi M\, d_F)^{-1}$ dependence as shown in the inset of Fig. 5(b).

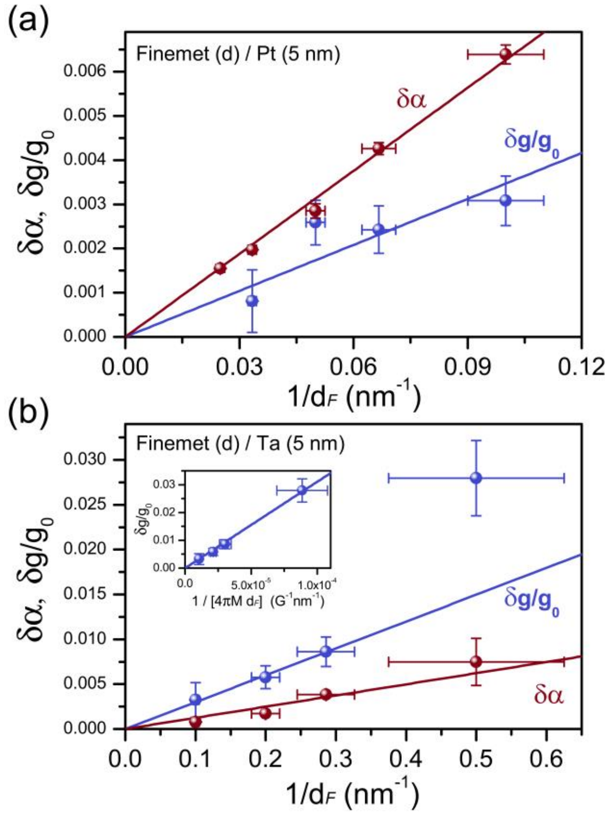


Fig. 5. Gilbert damping enhancement and a relative change in the $g$-factor due to spin pumping for Finemet|Pt (a) and Finemet|Ta (b). Solid lines are fits to the data according to Eqs. (3) and (4). The inset in (b) shows that $\delta g/g_0$ scales almost perfectly with $(4\pi M\, d_F)^{-1}$ if the magnetization of the film experiences serious changes with $d_F$ (see Eq. (4)).

## V. DISCUSSION

For Finemet|Pt bilayers our results nearly agree with those obtained by Mizukami et al. [5]. Keeping in mind that they had two interfaces (Pt|Permalloy|Pt), their study yields $\mathrm{Re}\left[g_{eff}^{\uparrow\downarrow}\right]$ and $\mathrm{Im}\left[g_{eff}^{\uparrow\downarrow}\right]$ equal to $3\times 10^{15} cm^{-2}$ and $0.6\times 10^{15} cm^{-2}$, respectively. For Finemet|Ta bilayers the impact of the Ta layer on damping is very reduced in comparison to Pt, in agreement with former studies [5,26,27]. The estimated real part of spin mixing conductance yielding $\mathrm{Re}\left[g_{eff}^{\uparrow\downarrow}\right]$ of $0.61\times 10^{15} cm^{-2}$, nicely coincides with earlier reports for Permalloy|Ta ($0.51\times 10^{15} cm^{-2}$) [5], $Co_2MnGe$|Ta ($0.55\times 10^{15} cm^{-2}$) [26] or for CoFeB|Ta ($0.54\times 10^{15} cm^{-2}$) [27] confirming that the weak damping enhancement for Ta arises from a small value of $\mathrm{Re}\left[g_{eff}^{\uparrow\downarrow}\right]$ [28].

In contrast, the results for the imaginary part of spin mixing conductance for Finemet|Ta bilayers show a different behavior than that observed by Mizukami et al. for Permalloy|Ta structures [5]. The impact of Ta on the $g$-factor results in a rather unexpectedly high value $\mathrm{Im}\left[g_{eff}^{\uparrow\downarrow}\right] = 1.61 \times 10^{15} cm^{-2}$. Their observations concerning the $g$-factor versus $d_{Py}$ are not confirmed by our measurements. Instead of a substantial down shift in the $g$-factor corresponding to $\mathrm{Im}\left[g_{eff}^{\uparrow\downarrow}\right] = -0.46 \times 10^{15} cm^{-2}$ (inferred from only one experimental point for thin Permalloy of 3 nm - see Fig. 6 in Ref. [5]), we see in Fig. 5 a regular behavior that can be nicely fit to Eq. (4). A high value of $\mathrm{Im}\left[g_{eff}^{\uparrow\downarrow}\right]$ leads to $\frac{\delta\alpha}{\delta g/g_0} = 0.38$. Figure 4 further confirms that the increase in the g-value for F|Ta bilayers is regular and saturates very fast for $d_{Ta} > 2$ nm.

Let us discuss the main results shown in Fig. 5 in terms of Eq. (9). For F|Pt bilayers $\frac{\delta\alpha}{\delta g/g_0} = 1.81$ what roughly gives $\frac{\bar{t}}{\tilde{\gamma}_{xz}} \approx 10$, i.e., $\tilde{\gamma}_{xz} \approx 100$ meV if we assume $\widetilde{t_\sigma^0} \approx 1$ eV after Ref. [11]. Our estimation of $\frac{\delta\alpha}{\delta g/g_0}$ (and hence the ratio $\mathrm{Re}\left[g_{eff}^{\uparrow\downarrow}\right]$ to $\mathrm{Im}\left[g_{eff}^{\uparrow\downarrow}\right]$) for F|Pt is in a rough agreement to the order of magnitude with those which we can infer from the results of Mizukami et al. [5] (≈ 5) or Nan et al. (≈ 3.8) for Permalloy|Pt [6]. In contrast, for F|Ta bilayers $\frac{\delta\alpha}{\delta g/g_0} = 0.38$. According to the microscopic analysis, this value suggests a strong spin-orbit contribution to the spin pumping effects. A rough estimation according to Eq. (9) gives an unreasonably high value of $\tilde{\gamma}_{xz}$ of the order of ≈ 700 meV.

A more thorough analysis allows us to estimate more precisely the strength of the hopping amplitudes $\widetilde{t_\sigma^0}$ and interface spin-orbit interaction $\tilde{\gamma}_{xz}$. By combining Eqs. (6) and (7) and posing $\frac{\widetilde{t_\sigma^0}}{\epsilon_F} = \tau_\sigma$ and $\frac{\tilde{\gamma}_{xz}}{\epsilon_F} = \eta$ (where the Fermi energy is $\epsilon_F \cong 1\, eV$), we arrive at a simple quadratic equation

$$s\,\tau_\sigma^2 - \frac{\delta g/g_0}{\eta}\tau_\sigma + \delta\alpha = 0, \tag{11}$$

where $s = a/d_F$, and $\sigma = \uparrow,\downarrow$. It is easily to show that for the F|Pt bilayers with: $s = 0.02$ ($d_F = 10\, nm$), $\delta g/g_0 = 3 \times 10^{-3}$ and $\delta\alpha = 6 \times 10^{-3}$, the real roots from a seeking region $\tau_\sigma \approx 1$ exists only for $\eta < 0.14$, i.e., $\tilde{\gamma}_{xz}$ of 130-140 meV. The same estimation for the F|Ta bilayers with $s = 0.1$ ($d_F = 2\, nm$), $\delta g/g_0 = 15 \times 10^{-3}$ and $\delta\alpha = 5 \times 10^{-3}$ gives $0.15 < \eta < 0.16$, i.e., $\tilde{\gamma}_{xz}$ of 150-160 meV since $\eta$ should also fulfill the conditions $\eta < \tau_\sigma$ and $\tau_\sigma \approx 1$. Having in mind our crude approximation of $\epsilon_F$ and $\tau_\sigma$, the values of the spin-orbit energy agree to the order of magnitude with that calculated by Cowan for 5d metals but with the reversed sequence of $\tilde{\gamma}_{xz}$ values in comparison with the spin-orbit parameters for Ta and Pt [29]. However, what is perhaps more important than a rough estimation of $\tilde{\gamma}_{xz}$ values, solutions of Eq. (11) (for $\tau_\sigma$) are almost equall for $\sigma = \uparrow, \downarrow$ in the case of F|Pt bilayers (i.e., $\widetilde{t_\uparrow^0} \approx \widetilde{t_\downarrow^0} \approx 0.5$), while they are strongly distinct for F|Ta (i.e., $\widetilde{t_\uparrow^0} \approx 0.1\widetilde{t_\downarrow^0}$). That is the reason of a low value of $\delta\alpha/(\frac{\delta g}{g_0})$ of 0.3 for the F|Ta bilayers. The origin of this effect requires further studies.

## VI. CONCLUSIONS

In conclusion, we have investigated the effect of spin pumping in Finemet films with wedge Pt and Ta capping layers. We explicitly showed the linear dependences of the Gilbert damping and the $g$-factor shift on the inverse Finemet thickness what allows us to determine both the real and imaginary part of spin mixing conductance. In particular, we showed that the spin pumping in the F|Ta bilayers is governed by a dominant role of $\mathrm{Im}\left[g_{eff}^{\uparrow\downarrow}\right]$ contributing to the field-like torque. The results were further discussed in terms of the microscopic spin pumping theory for metallic systems allowing for evaluation of the hopping amplitudes and the interface spin-orbit interaction.

## ACKNOWLEDGEMENTS

We acknowledge the support from the project "Marie Skłodowska-Curie Research and Innovation Staff Exchange (RISE)" Contract No. 644348 with the European Commission, as part of the Horizon2020 Programme.

## REFERENCES


[1] K. Sato, E. Saitoh, A. Willoughby, P. Capper, and S. Kasap, *Spintronics for next Generation Innovative Devices* (John Wiley and Sons, 2015).

[2] S. Azzawi, A. T. Hindmarch, and D. Atkinson, J. Phys. D. Appl. Phys. **50**, 473001 (2017).

[3] F. D. Czeschka, L. Dreher, M. S. Brandt, M. Weiler, M. Althammer, I. Imort, G. Reiss, A. Thomas, W. Schoch, W. Limmer, H. Huebl, R. Gross, and S. T. B. Goennenwein, Phys. Rev. Lett. **46601**, 46601 (2011).

[4] K. Xia, P. J. Kelly, G. E. W. Bauer, A. Brataas, and I. Turek, Phys. Rev. B **65**, 220401 (R) (2002).

[5] S. Mizukami, Y. Ando, and T. Miyazaki, Jpn. J. Appl. Phys. **40**, 580 (2001).

[6] T. Nan, S. Emori, C. T. Boone, X. Wang, T. M. Oxholm, J. G. Jones, B. M. Howe, G. J. Brown, and N. X. Sun, Phys. Rev. B **91**, 214416 (2015).

[7] Y. Sun, H. Chang, M. Kabatek, Y. Song, Z. Wang, M. Jantz, W. Schneider, M. Wu, S. G. E. Velthuis, H. Schultheiss, and A. Hoffmann, Phys. Rev. Lett. **111**, 106601 (2013).

[8] A. B. Cahaya, A. O. Leon, and G. E. W. Bauer, Phys. Rev. B **96**, 144434 (2017).

[9] K. Kim, K. Lee, J. Sinova, H. Lee, and M. D. Stiles, Phys. Rev. B **96**, 104438 (2017).

[10] M. Cecot, Ł. Karwacki, W. Skowroński, J. Kanak, J. Wrona, A. Żywczak, L. Yao, S. van Dijken, J. Barnaś, and T. Stobiecki, Sci. Rep. **7**, 968 (2017).

[11] G. Tatara and S. Mizukami, Phys. Rev. B **96**, 64423 (2017).

[12] Y. Tserkovnyak, A. Brataas, and B. I. Halperin, Rev. Mod. Phys. **77**, 1375 (2005).

[13] M. Zwierzycki, Y. Tserkovnyak, P. J. Kelly, A. Brataas, and G. E. W. Bauer, Phys. Rev. B **71**, 64420 (2005).

[14] H. Głowiński, I. Gościańska, A. Krysztofik, J. Barnaś, M. Cecot, P. Kuświk, and J. Dubowik, in *21st Int. Conf. Microwave, Radar Wirel. Commun. MIKON 2016* (2016).

[15] I. Gościańska, J. Dubowik, H. Ratajczak, M. Konc, and P. Sovak, J. Magn. Magn. Mater. **177**, 242 (2002).

[16] M. J. P. Alves, F. Bohn, and R. L. Sommer, J. Appl. Phys. **117**, 123913 (2015).

[17] D. R. G. Mitchell, Microsc. Res. Tech. **71**, 588 (2008).

[18] H. Głowiński, M. Schmidt, I. Gościańska, J. Ansermet, and J. Dubowik, J. Appl. Phys. **116**, 53901 (2014).

[19] P. Kuświk, H. Głowiński, E. Coy, J. Dubowik, and F. Stobiecki, J. Phys. Condens. Matter **29**, 435803 (2017).

[20] C. T. Boone, J. M. Shaw, H. T. Nembach, and T. J. Silva, J. Appl. Phys. **117**, 223910

(2015).
[21] A. Conca, S. Keller, L. Mihalceanu, T. Kehagias, G. P. Dimitrakopulos, B. Hillebrands, and E. T. Papaioannou, Phys. Rev. B **93**, 134405 (2016).
[22] J. M. Shaw, H. T. Nembach, T. J. Silva, and C. T. Boone, J. Appl. Phys. **114**, 243906 (2014).
[23] J. Bland and B. Heinrich, *Ultrathin Magnetic Structures IV: Applications of Nanomagnetism* (Springer, 2005).
[24] J. Brandao, S. Azzawi, A. T. Hindmarch, and D. Atkinson, Sci. Rep. **7**, 4569 (2017).
[25] J. Foros, G. Woltersdorf, B. Heinrich, and A. Brataas, J. Appl. Phys. **97**, 10A714 (2014).
[26] J. M. Shaw, E. K. Delczeg-Czirjak, E. R. J. Edwards, Y. Kvashnin, D. Thonig, M. A. W. Schoen, M. Pufall, M. L. Schneider, T. J. Silva, O. Karis, K. P. Rice, O. Eriksson, and H. T. Nembach, Phys. Rev. B **97**, 94420 (2018).
[27] G. Allen, S. Manipatruni, D. E. Nikonov, M. Doczy, and I. A. Young, Phys. Rev. B **91**, 144412 (2015).
[28] Y. Liu, Z. Yuan, R. J. H. Wesselink, A. A. Starikov, and P. J. Kelly, Phys. Rev. Lett. **113**, 207202 (2014).
[29] R. D. Cowan, *The Theory of Atomic Structure and Spectra, 3* (Univ of California Press, 1981).

Supporting Information

# Spin pumping effects in Finemet|Pt and Finemet|Ta bilayers: Influence of real and imaginary part of spin mixing conductance on magnetization dynamics.

A. Krysztofik, H. Głowiński, I. Gościańska and J. Dubowik*

*Institute of Molecular Physics, Polish Academy of Sciences, M. Smoluchowskiego 17, 60-179 Poznań, Poland*

E. Coy, K. Załęski

*NanoBioMedical Centre, A. Mickiewicz University, Umultowska 18, 60-614 Poznań, Poland*

*dubowik@ifmpan.poznan.pl

Contents:

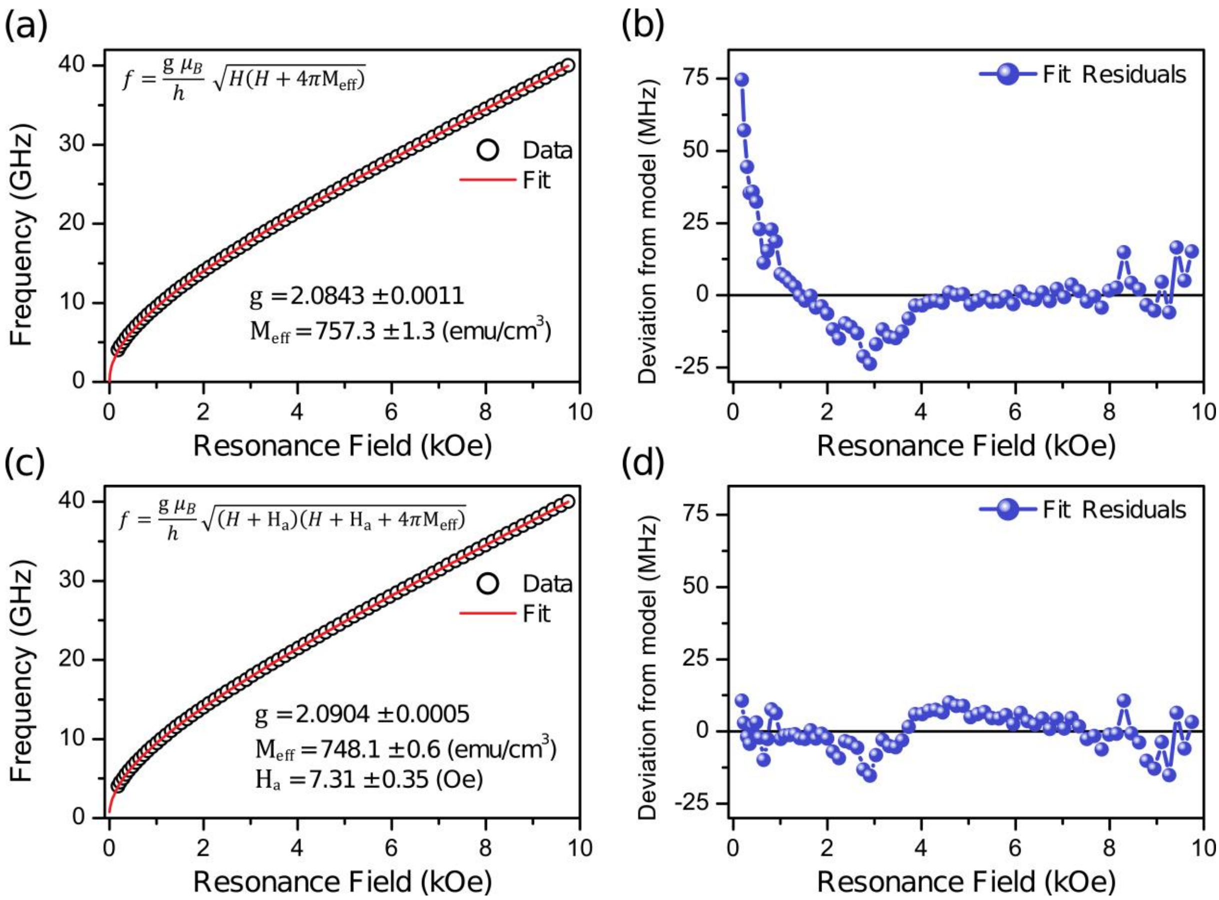


Fig. S1. Analysis of the residuals from a fitted dispersion models for 20 nm thick Finemet film. Residuals in (b) corresponds to the standard Kittel's model shown in (a). It is clearly seen that for resonance fields below 3 kOe residuals experience a monotonically increasing trend. Inclusion of anisotropy field in the model shown in (c) results in evenly distributed residuals displayed in (d). Note, that the fitted value of *g*-factor significantly differs between those two models.